

# Longwave 3D Benchmarks for Inhomogeneous Clouds and Comparisons with Approximate Methods

GEORGE P. KABLUCK III

*University of Maryland, College Park, College Park, Maryland*

ROBERT G. ELLINGSON

*The Florida State University, Tallahassee, Florida*

EZRA E. TAKARA

*Lockheed Martin Space Systems, Palo Alto, California*

JLUJING GU

*The Florida State University, Tallahassee, Florida*

(Manuscript received 26 March 2010, in final form 13 October 2010)

## ABSTRACT

The purpose of this study is twofold: to (i) establish three-dimensional (3D) longwave radiative transfer benchmarks for inhomogeneous cloud fields and (ii) compare the results with three approximate, 1D methods. The benchmark results are calculated using a correlated- $k$  three-dimensional Monte Carlo (3DMC) algorithm that is validated via comparisons to line-by-line calculations for simple atmospheres. The approximate methods include an independent column approximation (ICA) and two cloud-overlap schemes: maximum/random (MRO) and random (RO). Six inhomogeneous cloudy-sky test cases are used and encompass a wide range of domain sizes used by general circulation models. Domain-averaged fluxes and heating rates from these atmospheres show that the ICA is consistently more accurate than the cloud-overlap models with respect to the 3D benchmarks. For example, comparisons of model results for the Atlantic Trade Wind Experiment (ATEX), a marine boundary layer cumulus field, yield a maximum cloud-layer heating rate error of  $15.73 \text{ K day}^{-1}$  from using cloud-overlap models, whereas the ICA error is only  $2.17 \text{ K day}^{-1}$ . This paper presents results showing that these differences are attributed to the 3D effects of unresolved clouds and indicate that there is an inherent deficiency in the ability of 1D models to accurately calculate radiative quantities in these atmospheres.

## 1. Introduction and objectives

There is general agreement among atmospheric scientists that weak parameterization of interactions between radiation and clouds is responsible for much of the uncertainty in modeling the magnitude of anthropogenic influences on climate. Misrepresenting the spatial and temporal distribution of water in large-scale atmospheric models (LSAMs) will produce errors in calculated fluxes

that suggest unrealistic radiative forcings. The sensitivity and uncertainty in cloud effects on the earth's energy system are the motivation for many studies that seek to quantify the consequences of misrepresenting cloud radiative effects (Ellingson et al. 1991; Barker et al. 2003; Collins 2001).

Parameterizing gases, aerosols, and clouds is necessary for yielding climate-modeling results within the practical range of current computing power but in many cases is known to produce systematic errors (Räisänen 1998). Many studies have shown that the longwave irradiance contribution from cloud sides is significant to both surface fluxes and layer heating rates (chapter 6–10, Marshak and Davis 2005). Since LSAMs are relied upon to answer

---

*Corresponding author address:* George P. Kablick III, Dept. of Atmospheric and Oceanic Science, University of Maryland, College Park, MD 20742-2425.  
E-mail: pkablick@atmos.umd.edu

questions about climate change, errors in how radiation algorithms handle clouds must be minimized.

The research presented in this paper is the next step in the Intercomparison of Radiation Codes in Climate Models (ICRCCM) that was first published by Ellingson and Fouquart (1991) and more specifically is an extension of the third phase (ICRCCM III) performed by Barker et al. (2003). The first phase of ICRCCM focused on model performance for plane parallel homogeneous (PPH) skies and identified disparities as large as 40% among 1D models. For overcast longwave calculations, most models were in agreement at the cloud boundaries, but farther away from the clouds there were large differences. Optically thin clouds, for example, had net longwave flux differences of 35–80 W m<sup>-2</sup> at the vertical boundaries that resulted from how clouds were treated by the models (Ellingson et al. 1991).

Since that time, the Atmospheric Radiation Measurement (ARM) program has been working on validating model calculations against high-quality spectral observations taken at sites around the world (Stokes and Schwartz 1994; Ackerman and Stokes 2003). These data have helped develop accurate, line-by-line (LBL) information about atmospheric constituents, from which a line-by-line radiative transfer model (LBLRTM) has been established for model validation (Clough et al. 1992; Clough and Iacono 1995). This work has led to improvements in 1D model performance for clear and overcast skies; however, more research is needed to improve simulations that calculate radiative transfer through non-PPH skies (Turner et al. 2004).

Most 1D model disagreements have been resolved for simple atmospheres with the identification of errors in computational methods, acquisition of accurate spectral data, and calibration of radiation codes. However, certain biases remain due to implicit model characteristics such as cloud-overlap configurations. Studies testing the validity of cloud-overlap schemes show a strong dependence on vertical resolution and errors associated with neglecting horizontal fluctuations (Pincus and Klein 2000). Many researchers see the need to develop methods to improve the parameterization of unresolved clouds and 1D codes that incorporate them (Barker et al. 2003; Ackerman and Stokes 2003; Stephens 2005). New methods have been developed to replace cloud-overlap techniques used in LSAMs and many current climate models incorporate such methods (Morcrette et al. 2008; Pincus et al. 2006). However, cloud overlaps have yet to be tested against full 3D calculations in the longwave, and this study aims to provide the results necessary to more completely identify the deficiencies in the schemes.

ICRCCM III focuses on 1D model treatment of unresolved clouds. The objective of Barker et al. (2003)

was to achieve shortwave radiation benchmarks for broken cloud fields and assess the performance of 1D solar codes for these skies. The methods they examined include an independent column approximation (ICA), the maximum/random overlap (MRO), and random overlap (RO) cloud configurations. Their intercomparison included a total of 29 separate codes, four of which were 3D Monte Carlo (MC) and 25 were 1D models. They found that the ICA models performed better than single-column cloud-overlap configurations against MC benchmarks. However, that study also suggested that in deep layers of inhomogeneity, the ICA introduced significant errors in domain-averaged irradiance from neglecting cloud-side radiation. Their results also suggested that the use of extreme (and unrealistic) cloud-overlap schemes might falsely enhance cloud radiative forcing (CRF) by 20–50 W m<sup>-2</sup> in LSAM simulations.

The focus of this study is to extend ICRCCM III into the longwave spectral range. First, a correlated-*k* three-dimensional backward Monte Carlo model (3DMC) is validated and used to establish benchmarks for the same partially cloudy atmospheres used by Barker et al. (2003). Keeping with previous intercomparisons, the benchmark model is validated against line-by-line calculations for PPH conditions so that a baseline set of results can be established for more complicated scenarios—in this case, 3D inhomogeneous clouds. It is necessary to use 3DMC as a benchmark since it becomes computationally very difficult for LBL models to calculate a full set of results for the longwave while including the effects of multiple scattering.

Next, these results are compared to an independent column version of the MC code and the random and maximum/random cloud-overlap schemes incorporated by the rapid radiative transfer model (RRTM; Mlawer et al. 1997) to assess the performance of approximating real cloud situations. To be consistent with Barker et al. (2003), identical assumptions are made regarding the atmospheric distributions and properties of radiatively important variables. The following section discusses the four radiative transfer algorithms used, and sections 3 and 4 discuss the cases and the results of the intercomparison, respectively. The final section offers a summary and conclusions.

## 2. Models

In noncontiguous cloud fields, the effects of cloud-side radiation are not accounted for in atmospheric models with a two-stream approximation since horizontal transport is neglected. Real cloud situations have variable drop sizes and nonuniform layer densities that significantly alter the optical properties across the spectrum. This type of inhomogeneity presents more of a challenge for 1D models than the lack of PPH conditions. Since, by design,

3D radiation is neglected in single-column models, calculations for unresolved cloud fields will not produce results that exactly agree with observed fluxes above and below. Therefore, to achieve benchmark accuracy for inhomogeneous skies and to quantify the full effect of real clouds on radiation, multidimensional models must be used.

Three models are intercompared in this study; the 3DMC is used to set benchmarks for all cases and to test the accuracy of RRTM and a 1D version of the MC code (ICA). The ICA version allows for cloud inhomogeneity by calculating for a series of independent columns across the domain. RRTM is a good choice for this intercomparison since it has been validated against LBLRTM and has cloud-overlap parameterizations built into it (Mlawer et al. 1997). RRTM is employed with the maximum/random and the random cloud-overlap configurations, making a total of four algorithms. It is not an objective of this study to test cloud-generating schemes based on how they interpret observed cloud fractions but rather to test how established methods treat the radiative transfer, so using RRTM for the cloud-overlap calculations is appropriate.

The  $k$  distributions used by 3DMC, ICA, and RRTM are generated from the same spectral data in LBLRTM, so that there is no ambiguity in the results from the use of different spectral coefficients. Ellingson et al. (1991) demonstrated that testing the effects of different spectral data across various models calculating the same quantity is a study unto itself. Therefore, using the same spectral data for all models enables the geometric effects of clouds to be isolated more completely in the results. The rest of this section discusses the validation and implementation of 3DMC and presents an overview of the ICA and RRTM cloud overlaps.

#### *a. Monte Carlo benchmarks*

The Monte Carlo model used in this study is described in detail by Ellingson and Takara in chapter 10 of Marshak and Davis (2005). Briefly, the code uses a probabilistic simulator to compute radiative quantities from the statistics of many simulations of photon transport through a given atmosphere. At the core of these simulations is a pseudorandom number generator that determines all the events that can occur in the life of the photon. The simulations are based on the physical parameters of the particular atmosphere, using quantities such as temperature, water vapor, liquid water content, drop sizes, and other well- and nonwell-mixed gases to compute the transmission, absorption, and scattering. The statistics of these iterations converge to the true solution of how real photon energy behaves. The convergence criteria is a standard deviation test that determines when a unique solution has emerged from the results of individual photon transport.

For this study, the longwave spectrum is divided into 16 bands and each band contains 16 spectrally weighted absorption coefficients  $k$  such that there are 256 total  $k$  values. Optical properties of the model are handled with Mie scattering for cloud liquid water and a correlated- $k$  distribution to account for gaseous absorption (Li and Barker 2005). The exact 3D cloud field as generated by a cloud resolving model (CRM) is input to 3DMC with the assumption of periodic boundary conditions. The output is either the broadband estimate of irradiance or flux divergence for the entire grid.

One drawback of using MC is the large amount of computer time required for the computations, which makes it impractical for operational use in climate simulations. However, the time required to calculate the radiative transfer for one atmospheric scenario can be considerably reduced with the use of parallel processing. The MC model used here is based on the results of the Intercomparison of Three-Dimensional Radiation Codes (I3RC) (Cahalan et al. 2005) and has been formatted for a parallel-computing environment to decrease execution time. The advantages of using a parallel model are its ability to compute the fluxes and heating rates of any inhomogeneous cloud field with high accuracy and its relatively small memory requirements. Currently, runtime for 3DMC is on the order of a few hours for the entire longwave spectrum for a moderately sized inhomogeneous grid box  $\sim(75 \text{ km})^2$  with 50 vertical layers and 256 spectral intervals. Execution time, however, is highly dependent on specified input parameters like number of photon bundles per iteration, number of iterations per grid point, and convergence criteria. This MC model is quick enough for research purposes but is most likely too cumbersome for use in LSAMs.

3DMC model validation is performed with homogeneous, clear-sky comparisons to LBLRTM. LBLRTM was developed in conjunction with observations, and its high spectral accuracy makes it the benchmark standard for computing PPH fluxes (Clough et al. 1992; Clough and Iacono 1995). The spectral absorption coefficients from LBLRTM are sourced in RRTM to generate the correlated- $k$  distributions, so for simple atmospheres, RRTM closely agrees with LBLRTM to within  $0.6 \text{ W m}^{-2}$  per band for longwave net flux (Mlawer et al. 1997).

Clear-sky differences from LBLRTM and 3DMC are shown in Fig. 1, along with ICA and RRTM results. For this validation, the atmosphere from the tropical Barbados Oceanographic and Meteorological Experiment (BOMEX) case is used, but with the omission of cloud liquid water (see section 3 for more information on BOMEX). 3DMC and ICA are given a  $10 \times 10$  column patch of this cloudless atmosphere with PPH pressure, temperature, and gasses. The fluxes and heating rates

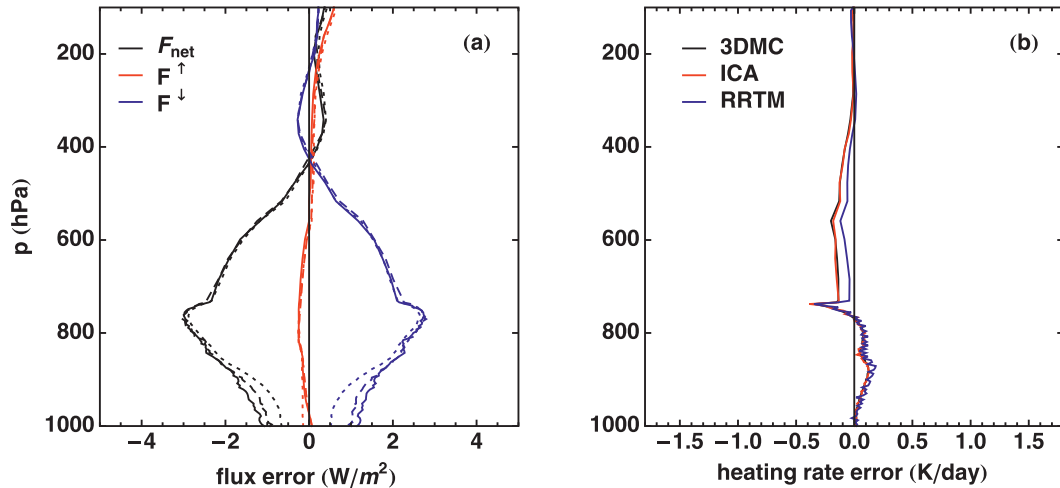


FIG. 1. Clear-sky 3DMC, ICA, RRTM, and LBLRTM comparison calculations for BOMEX. Shown here are the spectrally-integrated (a) flux errors for 3DMC, ICA and RRTM with respect to LBLRTM (3DMC, solid lines; ICA, dotted lines; RRTM, dashed lines) and the (b) corresponding heating rate errors.

are calculated for each column at all levels and then layer-averaged for comparison to LBLRTM. Averaging over a few columns smoothes over the random noise associated with MC calculations.

From an energy standpoint, the maximum differences are approximately  $3 W m^{-2}$  for downward flux  $F^\downarrow$  and less than  $0.5 W m^{-2}$  for upward flux  $F^\uparrow$ ; however, from a percentage standpoint, the error rarely exceeds  $\pm 2\%$ . The largest differences occur in the middle troposphere where the resolution is greatest (where cloud liquid water would be if it were included). However, at the surface and top-of-atmosphere (TOA;  $\sim 85$  km for these calculations), model differences are less than  $1 W m^{-2}$ . This performance for clear sky provides the necessary credibility for 3DMC's capabilities to properly calculate for inhomogeneous skies.

In the interest of making the model more efficient, another test is performed to determine if the number of photon bundle iterations used per  $k$  affects the spectrally integrated fluxes. As the model generates photon emission, it keeps track of the statistics of the calculated fluxes. Once the standard deviation of the computed quantity is within a predefined convergence criteria of 0.1%, the model averages the solutions that fall within that criteria and moves on to the next grid point. For this test, the code is run twice for a  $20 \times 20$  ( $1 km^2$ ) column cloudy-sky section of the BOMEX domain with both 2000 and 1000 photon iterations per  $k$ . The layer-averaged  $F^\downarrow$  for 1000 iterations is subtracted from that of 2000 iterations. The maximum difference is less than  $0.1 W m^{-2}$ , which is on the same order of magnitude as the noise introduced from the use of a pseudorandom number generator.

This test demonstrates that the differences in the two calculations are negligible and the convergence of a solution occurs before the 1000th iteration. However, individual convergence tests for each case were not conducted. Since the energy result for each  $k$  value is just the average of all the iterations performed, knowing the optimal number of iterations could significantly reduce the cost of computation. A more thorough examination of model efficiency may be a beneficial topic for future work.

#### b. Single-column models

All 1D radiation codes neglect certain properties of unresolved cloud structure via explicit assumptions that are meant to simplify calculations. The motivation for this simplification is a desire to speed up the computation process while retaining as much information as possible about the net fluxes and heating rates. Usually, 1D models assume infinitely wide clouds—an assumption that has been shown to impact global energy budget simulations (Kuhn 1978; Räisänen 1998; Collins 2001). In the presence of noncontiguous cloud fields that have variable liquid water amounts, radiation that crosses boundaries horizontally contributes significantly to the flux divergence of a particular column. When a grid box is approximated as independent, errors in radiative heating are introduced because the horizontal component of the flux divergence is being neglected. Perhaps if these biases are known, the codes can be calibrated to account for unrealistic radiative forcing at the surface and TOA.

The ICA was chosen for this intercomparison because of its potential as a replacement for radiation codes

currently employed by modern climate models. It has been shown to outperform 1D cloud-overlap models for many cases (Räisänen et al. 2004). The RO and MRO were chosen because they have traditionally been popular for use in climate simulations (Collins 2001). These three techniques are of interest to climate modelers that need a more accurate parameterization of cloud effect radiation.

### 1) ICA

In LSAMs, the grid box itself is usually the domain of an independent column calculation and “independent” refers to the isolation of radiation between adjacent columns. Conversely, the ICA is designed to preserve sub-grid inhomogeneity of cloud fields because it represents an areal distribution of 1D calculations, one for each grid point within a grid box. At each grid point, the ICA cloud fraction is assigned to be either 1 or 0, then the fluxes and heating rates are horizontally averaged to produce the results for the domain. Although this method eliminates the horizontal flow of radiation through the boundaries of the individual columns, it allows for the horizontal variability of clouds within the domain. ICA is useful for resolving the effects of multiple 1D radiative transfer calculations for domains that have substantial cloud variability and has been shown to be a vast improvement over 1D calculations that assume a PPH atmosphere for the entire grid box (Cahalan et al. 1994; Räisänen et al. 2004).

The ICA used herein is the full solution to the Monte Carlo independent column approximation (MCICA). MCICA has been developed to replace cloud-overlap techniques by stochastically generating cloudy columns for supplied cloud fractions and is currently implemented in many LSAMs (Pincus et al. 2003; Räisänen et al. 2004). Since the ICA is the full solution that MCICA approximates by averaging only a selection of columns, it is appropriate to include it in this study.

### 2) CLOUD-OVERLAP APPROXIMATIONS

The most common cloud-overlap method is the MRO scheme. Parameterizations using RO are increasingly rare, but it is included in this study for historical purposes since it was widely used in the past. The results of this intercomparison should be of interest to modelers that employ these schemes in single-column radiative transfer calculations (Räisänen 1998; Collins 2001). Iacono et al. (2000b) presented results from a comparison of these two overlap configurations used in the National Center for Atmospheric Research (NCAR) climate model that showed MRO decreases downward flux estimates over RO by about  $4 \text{ W m}^{-2}$  at the surface. MRO assumes maximum overlap of clouds occurring in consecutive layers and randomly overlaps clouds when separated by

two or more layers, whereas RO randomly aligns clouds without regard to vertical correlation. In both cases, the total cloud fraction  $N$  is preserved in individual cloud layers, but the different overlaps can result in largely different domain cloud fractions. It should also be noted that results obtained from overlap approximations depend upon the number of cloud layers present in the model, and this makes it difficult to intercompare similar treatment of clouds in LSAMs. For the cases in this study, all cloud-overlap calculations are performed by RRTM because it has been validated against LBLRTM and shares the  $k$  distributions with the MC models.

## 3. Cases

For consistency, the atmospheres used by Barker et al. (2003) are used in this study. Each case has significantly variable liquid water content (LWC) across the domain. Different resolutions and structures ensure that these cases encompass a wide range of inhomogeneity. Water vapor and all other atmospheric conditions except for liquid water are layer averaged, regardless of clear- or cloudy-sky location. This stipulation isolates the effect of liquid water on calculations and limits uncertainty from unchecked variables.

Cloud droplets are modeled as liquid water spheres with an effective radius  $r_e = 10 \mu\text{m}$ . This droplet size is chosen to be representative of average clouds since the main focus here is on the bulk, 3D geometric effects of clouds and not their physical properties. These clouds are quite opaque in the longwave region and have large liquid water paths (LWPs). Thus, changing  $r_e$  will not dramatically affect the fluxes. However, these results might not directly be applicable to clouds with smaller LWPs such as those found in the Arctic, so a future study might more thoroughly investigate variable  $r_e$ . See Kablick III (2008) for figures of the horizontal distribution of column-integrated LWP.

Where applicable, ice clouds are neglected because LSAM radiation codes do not treat ice optical properties uniformly. The physics of ice-radiation interaction is heavily dependent on crystal structure, and models vary in their treatment of ice optics or ignore it all together. The main objective of ICRCCM III was not to study microphysical effects on radiation model performance but to assess the handling of unresolved clouds in 1D models. Therefore, neglecting ice does not compromise the integrity of this study (Barker et al. 2003). The remainder of this section discusses individual cases in more detail.

The first case features a marine boundary layer stratocumulus field, simulated from conditions retrieved from the Atlantic Trade Wind Experiment (ATEX) of February 1969. The domain is  $6.8 \text{ km} \times 6.8 \text{ km}$  with

a horizontal gridspacing  $\Delta x = 0.1$  km. It has column-integrated LWP values ranging from 0–1.28  $\text{kg m}^{-2}$ . This type of cloud structure is predominant in trade regions of the tropics and is an important component of the general circulation. Stevens et al. (2001) explained that energy budget simulations are sensitive to the representation of low-level clouds associated with trade winds because they mediate energy transfer between the ocean surface and the atmosphere in the forms of latent and sensible heat. These regions are also important for zonal and meridional energy transport. Therefore, general circulation depends heavily on the physical interaction of radiation with these types of clouds.

The next field was generated by Siebesma and Cuijpers (1995) from data taken in BOMEX. Like ATEX, this CRM field contains marine cumuli in the trade wind region of the tropics. However, this cloud field is more sparse than ATEX, which makes a good test of the impact of different LWC with similar background conditions. The sparsity of liquid water in the BOMEX field means that there is less cloud radiative forcing than ATEX. It has the highest horizontal resolution used in this study with  $\Delta x = 0.05$  km over a domain of  $6.4 \text{ km} \times 6.4 \text{ km}$ , and the clouds did not originally contain any precipitation, so it did not have to be neglected for the calculations. BOMEX is discussed here because a clear-sky version of this atmosphere is used in 3DMC validation. The full results with the inclusion of clouds are not presented here. Those results, along with other cases, can be found in Kablick (2008).

Non-CRM-scale climate model grid boxes are on the order of  $(100 \text{ km})^2$  or more, so cloud fields of this dimension must be included in this intercomparison. A large-scale case was generated by Grabowski et al. (1998) from simulated conditions observed in the Global Atmospheric Research Program Atlantic Tropical Experiment (GATE A). This case has dimensions of  $400 \text{ km} \times 400 \text{ km}$  with  $\Delta x = 2$  km and contains clusters of deep convection. Clustering across the domain presents a problem for cloud-overlap configurations that depend on horizontally averaged values and assume an isotropic layer, so the results for this case are particularly noteworthy since it represents an extreme situation for cloud-overlapping methods.

This field was chosen because of its large-scale inhomogeneity and coarse resolution. The column-integrated LWP associated with this field is the most variable of all cases and has values ranging from 0–7.78  $\text{kg m}^{-2}$ . GATE A is the most computationally expensive case for 3DMC owing to its size. The grid spacing is large enough that 3DMC photon estimates may not be indicative of the entire grid point, so random perturbations are made to the simulations, such that 3DMC converges upon a more accurate solution.

## 4. Results and comparisons

This section details a sample of the 3DMC benchmarks, 1D model results, and the comparisons between them for ATEX and GATE A. Using 3DMC and ICA, the upward flux  $F^\uparrow$ , downward flux  $F^\downarrow$ , and heating rate  $q$  are computed independently at each 3D grid location. Using RRTM, the MRO and RO flux results are computed only as a function of height for a single column, and  $q$  is simply calculated from the change in net flux with respect to pressure derived from the model output of  $F^\uparrow$  and  $F^\downarrow$ . 3DMC and ICA results are layer averaged at the appropriate height before comparison to RRTM. Especially noteworthy, however, are nonaveraged 3DMC and ICA differences for individual atmospheric layers. Since ICA preserves the inhomogeneous cloud field, this comparison distinguishes the local forcing from 3D clouds. The remainder of this section discusses the benchmark results from 3DMC, compares the layer-averaged values for all models, and reviews the nonlayer-averaged 3DMC-ICA differences.

### a. 3D cloud-layer heating

The ATEX case is a good example of the longwave distribution of heating/cooling within a marine boundary layer cloud field. There is strong warming below the cloud where there is a net convergence of flux from the surface below and from the cloud above. The cooling aloft is indicative of the increase in net divergence as a result of decreasing downward flux with altitude. Figure 2a shows the 3DMC heating rate distribution for the ATEX cloud layer with cooling as low as  $-628 \text{ K day}^{-1}$  for individual grid points. This is an extreme value that is not indicative of the entire layer but rather a result of calculating flux divergence over a very small volume.

The 3D heating structure for GATE A is more difficult to visualize because the resolution is coarse. A single heating rate value for a grid point with a horizontal area of  $(2 \text{ km})^2$  produces a heating distribution that appears more random when viewed in the context of the whole domain because a single value may not be indicative of the entire grid point. Figure 2 shows cloud-layer heating for GATE A. The heating rates are calculated from flux divergences that are computed over larger volumes ( $\Delta x = 2$  km), which tend to decrease the extreme values at individual grid points as seen in ATEX. This effect of cloud geometry explains why the cooling is reduced to a minimum of  $-47 \text{ K day}^{-1}$ .

The differences in 3D heating rates for ATEX and GATE A demonstrate that low resolution plays a role on muting the impact of 3D clouds. The column-integrated LWP for GATE is much higher than ATEX, yet the cloud-layer heating is an order of magnitude lower. The

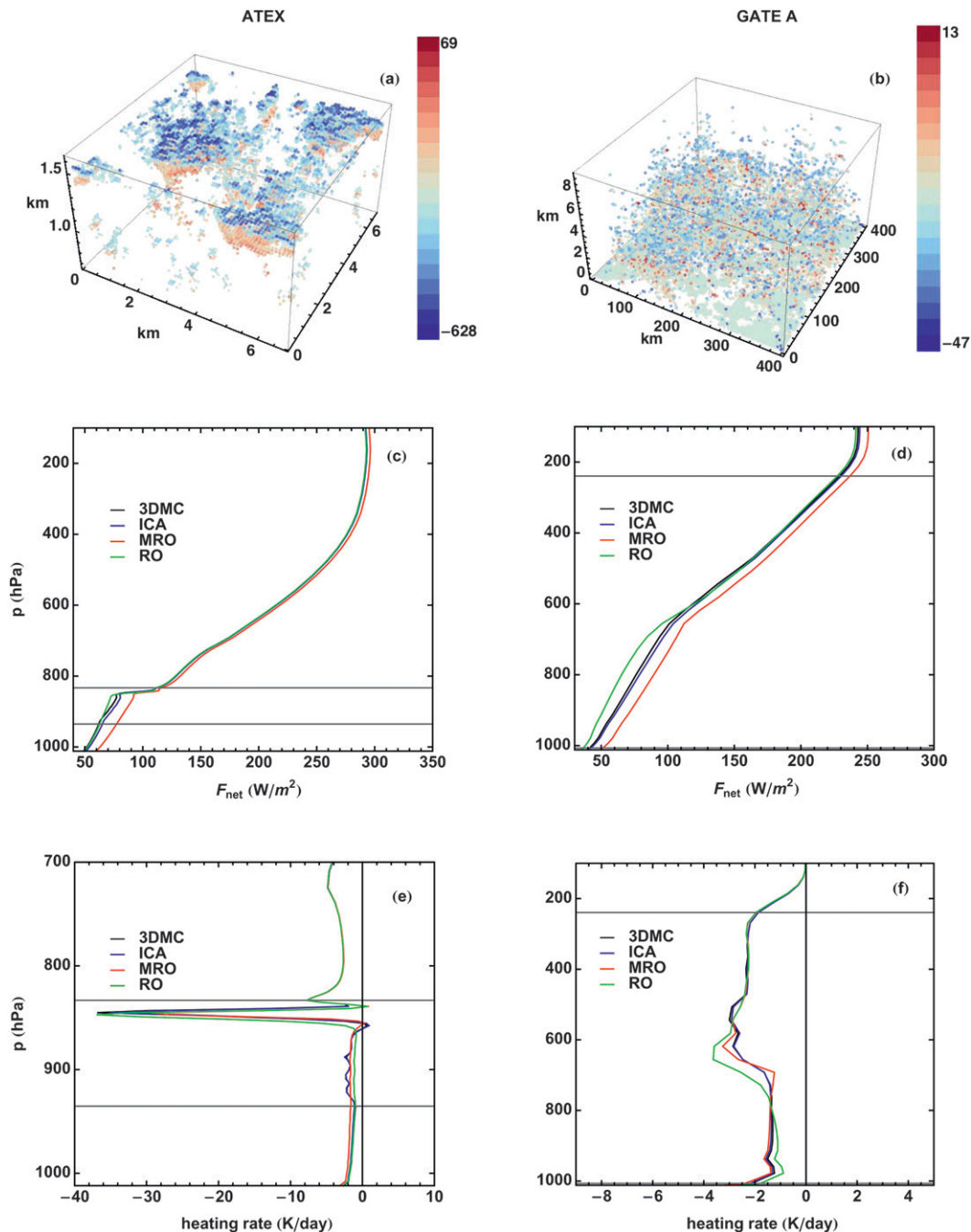


FIG. 2. (left) ATEX results showing (a) the 3DMC heating rate distribution ( $K \text{ day}^{-1}$ ), (c) domain-averaged net fluxes  $F_{net}$ , and (e) heating rates from each model. (right) As in (a), (c), (e), but for (b), (d), (f) GATE A. The horizontal gray lines in this figure represent the vertical boundaries of the cloud layer. Note for GATE A, the bottom of the cloud layer is near the surface.

effects of this limitation can be significant to cloud evolution in circulation models.

### b. Layer-averaged results

The layer-averaged vertical profiles for 3DMC net flux  $F_{net}$  and  $q$  for both cases are shown in Figs. 2c–f, where

longwave  $F_{net}$  is defined as  $F^{\uparrow} - F^{\downarrow}$ . Also shown are the approximate model results from ICA, MRO, and RO. Horizontal gray lines in the figure delineate the vertical boundaries of the cloud layer, which for ATEX is 935–833 hPa and for GATE A is 1006–240 hPa. Figures 2c and 2d indicate that for  $F_{net}$  the models are in fairly good

agreement above the cloud layer with MRO as the outlier in both cases.

An instructive way to interpret these results is in the framework of an effective cloud fraction  $N_e$  and how it relates to  $F^\downarrow$  and  $F^\uparrow$ . The upward or downward flux at a given level may be written as

$$F^{\uparrow\downarrow} = F_{\text{clear}}^{\uparrow\downarrow} + N_e(F_{\text{cloud}}^{\uparrow\downarrow} - F_{\text{clear}}^{\uparrow\downarrow}), \quad (1)$$

where  $N_e$  is the effective cloud fraction for either the sky above the level for  $F^\downarrow$  or below the level for  $F^\uparrow$ , and  $F_{\text{clear}}^{\uparrow\downarrow}$  and  $F_{\text{cloud}}^{\uparrow\downarrow}$  are the respective clear- and overcast-sky fluxes at the level of interest (Taylor and Ellingson 2008). In this framework,  $N_e$  can be interpreted as the PPH cloud fraction necessary to match the results of 3DMC. For the cases considered here,  $F_{\text{cloud}}^\uparrow < F_{\text{clear}}^\uparrow$  and  $F_{\text{cloud}}^\downarrow > F_{\text{clear}}^\downarrow$ . Thus, when  $F^\uparrow$  from an approximate model is less than 3DMC,  $N_e$  is too large, and when the approximate result is greater than 3DMC,  $N_e$  is too small. Likewise for downward flux comparisons, when  $F^\downarrow$  is less than 3DMC,  $N_e$  is too small, and when  $F^\downarrow$  is greater than 3DMC,  $N_e$  is too large. This discussion assumes that the clear- and overcast-sky fluxes are the same for each model, which is appropriate for three reasons: all models 1) treat clouds as blackbodies, 2) use PPH temperature and gases, and 3) show small differences between fluxes for the clear-sky validation.

In the case of MRO, clouds occurring in consecutive layers are maximally overlapped, which results in a smaller  $N_e$  for those layers across the domain as compared to 3DMC because cloud sides are neglected. The effect of this smaller cloud fraction results in an increased upward flux within and above the cloud layer and a smaller downward flux within and below the cloud layer. This result is consistent with Iacono et al. (2000a), who found MRO decreased  $F^\downarrow$  at the surface compared to RO. There is a decrease in RO  $F_{\text{net}}$  within the cloud layer because the random alignment of all cloud layers produces a larger  $N_e$  relative to MRO and thus a larger  $F^\downarrow$ .

At altitudes higher than the clear layers immediately above the uppermost cloud layer, heating rates are dominated by the divergence of clear-sky  $F_{\text{net}}$  (i.e., cooling to space). The difference between approximate results and 3DMC is governed by the product of the difference in  $N_e$  and the divergence of the difference between  $F_{\text{clear}}^\uparrow$  and  $F_{\text{cloud}}^\uparrow$ . Figures 2e and 2f show the model results for  $q$ . As indicated in this figure, all models agree quite well on the amount of cooling above the cloud layer because cooling in this region is dominated by clear-sky cooling to space as noted above. Near the top of the ATEX layer and near the middle of the GATE A layer is where the largest heating rate errors occur because  $N_e$  above and below the layer changes at different rates for each approximation. To fully glean the effects, it is

necessary to look at the differences between the approximate and exact  $F^\uparrow$ .

As expected, RRTM cloud-overlap results disagree among themselves; however, there is a surprising result in that RO performs better than MRO for every flux calculation with respect to the benchmarks. The differences occur because of the differences in the change of effective cloud fraction with height calculated by MRO and RO. This result is opposite of what was expected and is directly affected by the inherent sensitivity of cloud-overlap approximations to vertical resolution. Räisänen (1998) showed that MRO accuracy can be adversely affected by high vertical resolution. Although MRO performs poorly for these cases, it was not expected that the RO would perform as well as it did. In general, RO flux errors at all vertical locations are less than MRO, but the  $q$  errors are slightly greater. MRO errors in cloud-layer heating are smaller than RO because changes in net flux with altitude are less dramatic. RRTM and layer-averaged ICA errors are shown in Figs. 3a and 3c for fluxes and Figs. 3b and 3d for  $q$ . The largest differences between the two overlap approximations occur in the areas bound by the cloud layer.

ATEX has  $N = 0.565$  for the domain and 32 levels within a cloud layer that extends from 1.66 to 2.64 km in altitude. The vertical resolution through the cloud layer ranges from 0.02–0.04 km, so it would seem safe to assume the presence of clouds in consecutive layers this thin are the same cloud in space. However, ATEX has high-resolution horizontal grid spacing ( $\Delta x = 0.1$  km), so overlapping the clouds maximally into one column will result in errors because it assumes one column will be indicative of the entire, inhomogeneous grid. As seen in Fig. 3a for ATEX and Fig. 3c for GATE A, RO performs better than MRO for  $F^\downarrow$  near the surface. For the ATEX case, RO closely agrees with the 3DMC to within  $0.5 \text{ W m}^{-2}$  and the ICA to within  $2 \text{ W m}^{-2}$ , whereas MRO is approximately  $10 \text{ W m}^{-2}$  less than all three of these models.

Higher resolutions, coupled with variable-layer cloud fraction produce more total cloud coverage with RO than with MRO. If there are more, rather than fewer, adjacent cloud layers, it is more probable for a sky to appear overcast with random alignment than with maximum/random alignment. Therefore, the flux discrepancies make sense because a single column would have more downwelling irradiance beneath and less upwelling irradiance above a cloud layer if it had a higher total cloud fraction, which is the case with RO. Concurrently using MRO for a cloud field with high spatial resolution results in an underestimation of  $F^\downarrow$  at the surface because the vertical correlation decreases  $N_e$  as compared to the 3DMC.

These results can be interpreted in terms of how  $N_e$  changes with respect to cloud overlaps in each layer. For

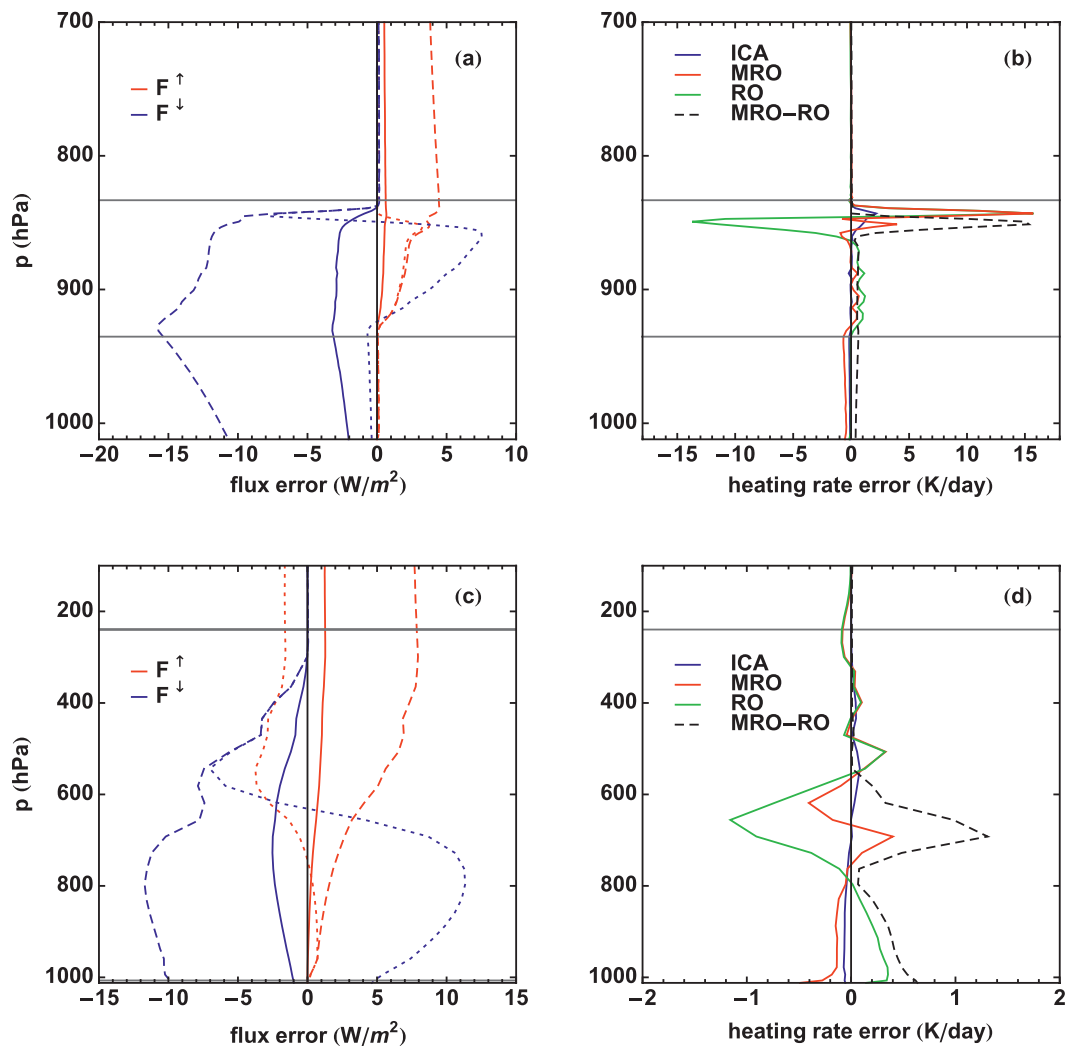


FIG. 3. The respective flux and heating rate errors (model-3DMC) for (a),(b) ATEX and (c),(d) GATE A. The error profiles in (a) and (c) are to be interpreted as ICA, solid lines; MRO, dashed lines; RO, dotted lines. Also (b),(d) show the differences between MRO and RO. The horizontal lines are the vertical cloud-layer boundaries.

the ATEX case, the 3D effect of clouds is to increase  $N_e$  below the cloud top, thereby contributing more  $F^\downarrow$ . In other words, the 3D effective cloud fraction is greater than the cloud fraction used by the cloud overlaps in this layer. However, just below the initial cloud levels, RO  $F^\downarrow$  increases dramatically because the random overlap of clouds above quickly increases the overcast fraction of sky. Further down in the cloud layer, 3DMC  $F^\downarrow$  is in better agreement with RO because the 3D geometric effects of clouds produce a  $N_e$  closer in value to RO cloud fraction. This result is a direct consequence of 3DMC's inclusion of emission from cloud sides.

This reasoning also explains why MRO flux errors appear more constant with altitude. An effect of MRO vertically aligning clouds in consecutive layers is that it has a smaller  $N_e$  than RO beneath layers of consecutive

clouds for the same conditions. This effect is enhanced when the vertical resolution is high, and the result is that MRO  $N_e$  is less likely to change with altitude. Below the cloud layer itself, the mitigating effects of atmospheric absorption decreases the errors. Similar situations for the GATE A fluxes are shown in Fig. 3c.

For  $F^\uparrow$ , it is clear that the 3D effects are not as strong since the errors are smaller than for  $F^\downarrow$ . This result can be attributed to the smaller differences between clear- and cloudy-sky  $F^\uparrow$ . Viewed from above, the surface and cloud layers have fluxes that are similar in magnitude because they are emitting at relatively similar temperatures. In contrast, when viewed from below, the magnitude of the fluxes in clear and cloudy skies is much different because downward emission by the clouds dominates the clear-sky emission in the atmospheric window regions.

The heating rate errors also demonstrate 3D effects. Figure 3b shows that for ATEX, MRO and RO are in close agreement near the top of the cloud layer as they both have large errors near  $15 \text{ K day}^{-1}$  but quickly differ below this level. The cloud overlaps underpredict cooling near the top of the cloud layer as a result of misrepresenting  $N_e$ . As shown in Fig. 3a, the RO  $F^\uparrow$  error in this region quickly changes from approximately 0 to  $3 \text{ W m}^{-2}$  just below the top of the cloud layer while the  $F^\downarrow$  error decreases from 0 to  $-8 \text{ W m}^{-2}$  and then rapidly increases to near  $7.5 \text{ W m}^{-2}$ . This rapid shift in the flux errors occurs because the actual cloud fraction is misrepresented through random cloud alignment. This results in the large  $q$  error. Just beneath this region in the cloud layer, MRO is in closer agreement to 3DMC because of similar values of flux divergence, but RO strongly overpredicts the cooling (near  $-15 \text{ K day}^{-1}$ ) because of the large decrease in  $F^\uparrow$  with height. Below this level, however,  $q$  errors quickly diminish as 3D effects compensate for the large  $N_e$  generated by RO. Similar effects are seen for the GATE A case (see Fig. 3d).

In general, the cloud overlaps do not perform as well as the ICA, but they perform better for the deep convection in GATE A where the clouds and the domain have greater dimensions. This is because the cloud properties for an individual column are more indicative of the domain-averaged values that RRTM computes. Therefore, the single-column RRTM results have less discrepancy compared to the benchmarks when  $\Delta x$  is large. The vertical locations of differences between MRO and RO are directly caused by the misrepresentation of 3D  $N_e$ . These calculations would most likely produce better results by using layer effective cloud fractions as input into RRTM instead of the simple fraction of cloudy- to clear-sky grid points. This might be done by combining the known CRM liquid water content at each layer with an assumption about cloud geometry to create a scene that is more representative of 3DMC  $N_e$ . However, such approximations have only been developed for some simple cloud cases (Han and Ellingson 2000), and more research is necessary before such parameterizations can be trusted.

Table 1 summarizes the layer-averaged model errors for downward flux at the surface  $F_{\text{sfc}}^\downarrow$  and the bottom of the cloud layer  $F_{\text{cb}}^\downarrow$ , upward flux at the top of the cloud layer,  $F_{\text{ct}}^\uparrow$  and TOA  $F_{\text{TOA}}^\uparrow$ , and the extrema in the cloud-layer heating rate error  $q_{\text{max}}$  as compared to 3DMC. For these results, TOA is  $\sim 85 \text{ km}$  in altitude.

### c. Boundary effects of 3D radiation

It is clear how locally important cloud-side radiation is when one views the areal distribution of  $F_{\text{sfc}}^\downarrow$  and  $F_{\text{TOA}}^\uparrow$ . Figure 4 shows apparent radiational smoothing along the boundaries of the clouds for both ATEX and GATE A.

TABLE 1. Comparison of model flux and heating rate errors. Listed here are the model errors for domain-averaged downward flux at the surface  $F_{\text{sfc}}^\downarrow$  and the bottom of the cloud layer  $F_{\text{cb}}^\downarrow$ , upward flux at the top of the cloud layer  $F_{\text{ct}}^\uparrow$  and TOA  $F_{\text{TOA}}^\uparrow$ , and the extrema in cloud-layer heating rate error  $q_{\text{max}}$  between the 1D models and 3DMC. All values of flux in  $\text{W m}^{-2}$  and heating rate in  $\text{K day}^{-1}$ .

Case	Model	Domain-averaged model errors				
		$F_{\text{sfc}}^\downarrow$	$F_{\text{cb}}^\downarrow$	$F_{\text{ct}}^\uparrow$	$F_{\text{TOA}}^\uparrow$	$q_{\text{max}}$
ATEX	ICA	-2.041	-3.130	0.622	0.448	2.17
	MRO	-10.682	-15.383	4.436	3.124	15.71
	RO	0.381	-0.680	0.039	-0.124	15.73
GATE A	ICA	-0.988	-1.020	1.264	1.176	0.09
	MRO	-9.678	-9.901	7.854	7.214	-0.49
	RO	4.624	4.800	-1.614	-1.687	-1.16

Figures 4a and 4b are ATEX  $F_{\text{sfc}}^\downarrow$  and  $F_{\text{TOA}}^\uparrow$ , respectively. Here,  $F_{\text{sfc}}^\downarrow$  is enhanced in clear skies along the boundaries of clouds, but the narrow dimensions of this domain combined with the low-altitude cloud layer cause less dramatic variations in  $F_{\text{TOA}}^\uparrow$ . Figures 4c and 4d show the boundary fluxes for GATE A. Figure 4c shows the same smoothing effects as seen in ATEX for  $F_{\text{sfc}}^\downarrow$ , but GATE A has larger variations in  $F_{\text{TOA}}^\uparrow$  because of the larger differences between the clear-sky and cloud-top fluxes.

Radiational smoothing is an effect that is not captured by traditional 1D models. Comparing 3DMC to ICA on a column-by-column basis shows large differences that are attributed to boundary-crossing photons. Although it prescribes  $N = 0$  or 1 at each column, ICA preserves the CRM cloud structure on the scale of the LSAM grid box. This allows for distinction of 3D cloud effects and provides insight into the local CRF from neglecting multidimensional radiation. Individual layer differences between 3DMC and ICA are shown in Fig. 5 for  $F_{\text{sfc}}^\downarrow$  and  $F_{\text{TOA}}^\uparrow$ . For all cases, the ICA has less  $F_{\text{sfc}}^\downarrow$  just outside the cloud boundaries and an increase inside the cloud as compared to 3DMC benchmarks. Figure 5a shows that ATEX  $F_{\text{sfc}}^\downarrow$  is increased by as much as  $39 \text{ W m}^{-2}$  in clear-sky columns and decreased by  $38 \text{ W m}^{-2}$  in cloudy columns.

Allowing the photons to have horizontal paths allows them to occasionally escape the column where they were generated. This is the main significance of 3D effects: photons can be scattered or emitted into adjacent columns and contribute to the flux. This can also be seen in Fig. 5b, where the ICA underpredicts the amount of upward flux and flux divergence from the cloud tops because it neglects horizontal transport. This figure shows that ATEX  $F_{\text{TOA}}^\uparrow$  is underestimated by as much as  $11 \text{ W m}^{-2}$  directly over the cloud tops and overestimated by  $10 \text{ W m}^{-2}$  over clear skies.

Figure 5c shows the  $F_{\text{sfc}}^\downarrow$  differences for GATE A. As seen in this figure, ICA underestimates  $F_{\text{sfc}}^\downarrow$  by as much

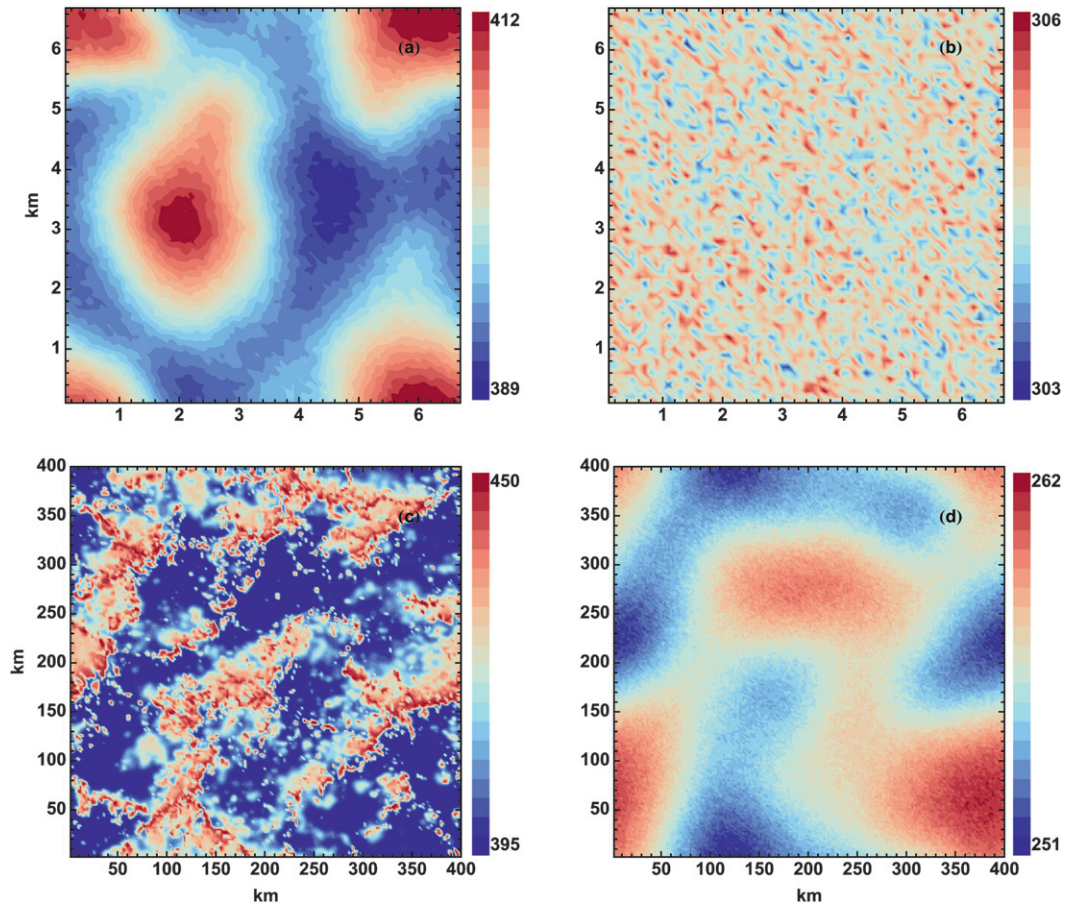


FIG. 4. The 3DMC benchmark results for ATEX (a)  $F_{\text{surf}}^{\downarrow}$  and (b)  $F_{\text{TOA}}^{\uparrow}$  and GATE A (c)  $F_{\text{surf}}^{\downarrow}$  and (d)  $F_{\text{TOA}}^{\uparrow}$ . All flux values in  $\text{W m}^{-2}$ . For these results, TOA is  $\sim 85$  km.

as  $34 \text{ W m}^{-2}$  just outside the cloud boundaries and overestimates by  $27 \text{ W m}^{-2}$  within the cloud boundaries. These differences are not as large as those for ATEX and are due in part to the coarse resolution of the domain. Figure 5d shows the difference in  $F_{\text{TOA}}^{\uparrow}$ . The upward-moving photons from clouds are more likely to cross into adjacent columns when viewed from higher up and in this case create differences up to  $100 \text{ W m}^{-2}$ . The deep inhomogeneity of GATE A combined with the large domain result in larger differences at TOA than ATEX because photons have a higher chance of contributing to flux in adjacent columns. Also, in clear skies there is a  $-19 \text{ W m}^{-2}$  difference in  $F^{\downarrow}$  where 3DMC sees not just the cold tops but also the cold sides of clouds. The ICA does not see this influence and therefore overestimates  $F^{\downarrow}$  in clear skies.

These differences are to be expected from the standpoint of individual columns. However, from a domain-averaged standpoint, these differences are significantly reduced. For all cases (including those not discussed here), the mean  $F_{\text{surf}}^{\downarrow}$  error for ICA is only  $-2.041 \text{ W m}^{-2}$ . ICA

also performed well for domain-averaged heating rate, with a mean error slightly larger than 2% and a maximum difference of  $2.17 \text{ K day}^{-1}$ , which occurred in the cloud layer.

## 5. Summary and conclusions

The objectives of this study have been to establish longwave inhomogeneous cloud field benchmarks using a 3DMC and to compare the performance of four approximate radiative transfer algorithms. Validation of 3DMC against a high-quality LBLRTM for simple atmospheres has given confidence in its ability to accurately compute 3D radiative transfer in real cloud scenarios. The approximate methods include an ICA, RO, and MRO. The full 3D comparisons are presented for only two of the cases (ATEX and GATE A) used in the shortwave ICRCM III (Barker et al. 2003). The full results and descriptions for other cases can be found in Kablick (2008).

Many LSAMs currently employ 1D radiation schemes that operate on domain-averaged values of gases, aerosols,

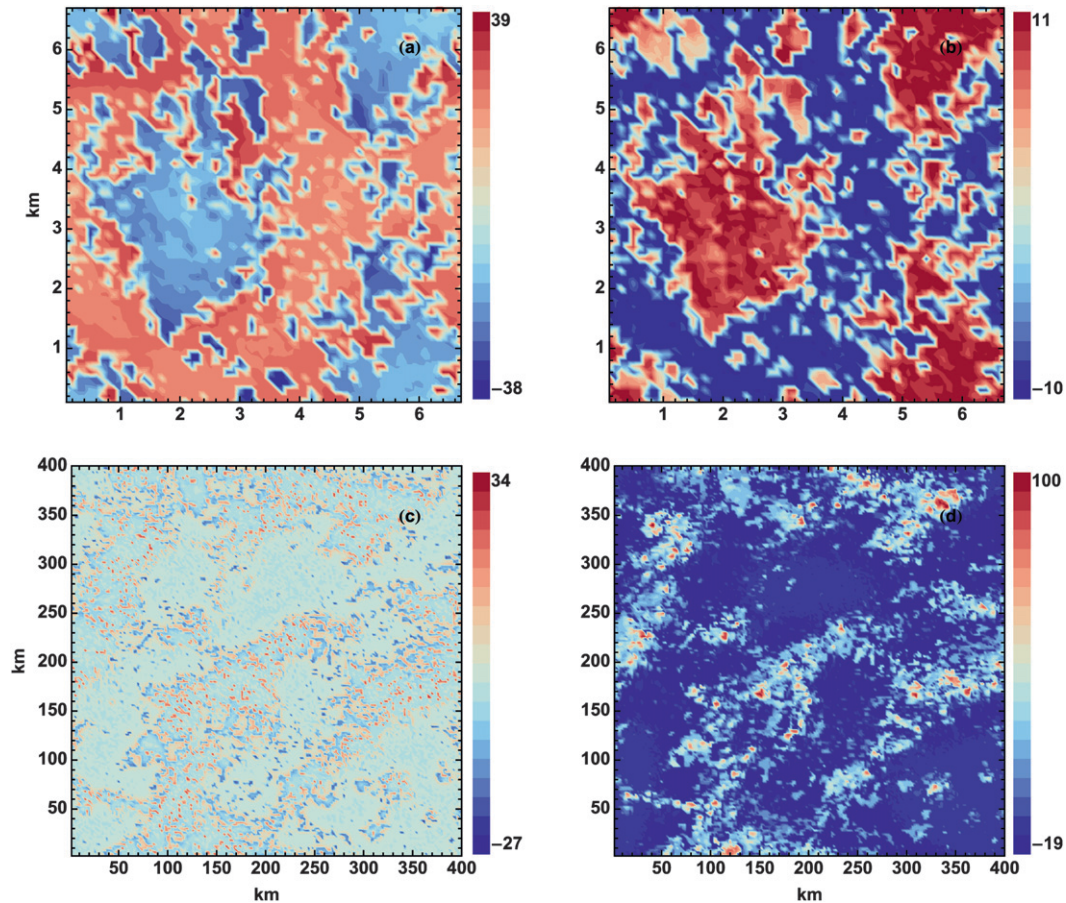


FIG. 5. The ICA individual column results subtracted from 3DMC for ATEX (a)  $F_{\text{sfc}}^{\downarrow}$  and (b)  $F_{\text{TOA}}^{\uparrow}$  and GATE A (c)  $F_{\text{sfc}}^{\downarrow}$  and (d)  $F_{\text{TOA}}^{\uparrow}$ . All flux values in  $\text{W m}^{-2}$ .

and clouds, and assume either RO or MRO for cloud-layer configuration. Comparing RO and MRO 1D methods to the 3D benchmark calculations has shown that, on average, the differences are great enough to cause unrealistic radiative forcing in LSAMs. Considering that  $10 \text{ W m}^{-2}$  forcing at the surface of the ocean can raise the surface temperature by 1 K over the course of a year (assuming a 75-m deep mixed layer), the sensitivity of climate might easily be misinterpreted if radiative transfer errors are not minimized (National Research Council 1982). Therefore, climate model simulations that employ PPH atmospheres and neglect 3D cloud effects can be a source of significant uncertainty in climate change scenarios. The identification of these discrepancies should help develop more accurate 1D methods, so that they can account for multidimensional radiation from unresolved clouds and reduce systematic errors in climate simulations.

The results from the approximate models are in close agreement with the 3DMC for clear layers above the cloud with MRO as an exception; however, there are large differences that occur inside and below layers that

contain liquid water. For the most part, the ICA performs better than the cloud-overlap approximations. The nature of ICA is to preserve the CRM cloud structure by independently assigning a value  $N = 0$  or 1 at each column, whereas the cloud-overlap methods assume horizontal approximations (i.e., neglect inhomogeneity) that tend to misrepresent realistic cloud configurations. ICA comes close to the benchmark because it successively averages each independent column that may have large under- and overpredictions across the domain, thereby converging on the 3D solution. Therefore, it can be concluded that resolving horizontally inhomogeneous clouds, although locally overcast ones, more accurately represents the atmosphere than using overlapping fractional clouds in one column. This result is consistent with the findings of the shortwave ICRCCM III, in which ICA models outperformed the cloud-overlap models (Barker et al. 2003).

Outside of the results presented here, the most promising 1D algorithm is MCICA (Pincus et al. 2003; Räisänen et al. 2004). The implementation of the MCICA sampling method is a useful way to achieve accurate results

with reduced computation time. It uses a correlated- $k$  distribution technique that is known for being quick and accurate for inhomogeneous atmospheres. The MCICA column-sampling method has also been praised for its speed over the standard ICA without a great loss in accuracy. The ICA results presented herein, however, are the full solution to the MCICA scheme, and thus, the benchmark to which MCICA can be compared. Therefore, it would be a worthy approximate method to test with these results in a future study.

The results shown herein are but for a few selected cases and are only a sample of cloud types found globally. The authors certainly agree with one of the reviewers of this manuscript that a beneficial future study would be to generate 3D cloud scenes from observational data and examine the differences between 3D and 1D for different variables (e.g., season, meteorological regime, latitude, land/ocean, etc.). This has been done by Cole et al. (2005) to some extent. Though that study was global, it incorporated 2D, not 3D clouds, and relied on CRM generated cloud fields.

In a similar fashion to previous intercomparisons, this study was not designed to be a unilateral effort. All of these results are available to other modelers who wish to participate in this intercomparison or to use the 3D benchmarks to validate their codes. Including more models in this intercomparison would broaden the range of results. The original scope of this project was to include as many established climate radiation methods as possible and various techniques that are in development that eventually might be included in climate model radiation packages.

*Acknowledgments.* The authors wish to thank the reviewers for comments and suggestions on improving the original manuscript as well as insightful topics for future research related to this work. This research was supported by the Office of Biological and Environmental Research of the U.S. Department of Energy under Grant Number DE-FEG02-02ER63338 as part of the Atmospheric Radiation Measurement Program.

#### REFERENCES

- Ackerman, T., and G. Stokes, 2003: The atmospheric radiation measurement program. *Phys. Today*, **56**, 38–44.
- Barker, H., and Coauthors, 2003: Assessing 1D atmospheric solar radiative transfer models: Interpretation and handling of unresolved clouds. *J. Climate*, **16**, 2676–2699.
- Cahalan, R., W. Ridgway, W. Wiscombe, and S. Gollmer, 1994: Independent pixel and Monte Carlo estimates of stratocumulus albedo. *J. Atmos. Sci.*, **51**, 3776–3790.
- , and Coauthors, 2005: The International Intercomparison of 3D Radiation Codes (I3RC): Bringing together the most advanced radiative transfer tools for cloudy atmospheres. *Bull. Amer. Meteor. Soc.*, **86**, 1275–1293.
- Clough, S., and M. Iacono, 1995: Line-by-line calculation of atmospheric fluxes and cooling rates 2: Application to carbon dioxide, ozone, methane, nitrous oxide and the halocarbons. *J. Geophys. Res.*, **100**, 519–16.
- , —, and J. Moncet, 1992: Line-by-line calculation of atmospheric fluxes and cooling rates: Application to water vapor. *J. Geophys. Res.*, **97**, 15 761–15 785.
- Cole, J., H. Barker, W. O. Hirok, E. Clothiaux, M. Khairoutdinov, and D. Randall, 2005: Atmospheric radiative transfer through global arrays of 2D clouds. *Geophys. Res. Lett.*, **32**, L19817, doi:10.1029/2005GL023329.
- Collins, W., 2001: Parameterization of generalized cloud overlap for radiative calculations in general circulation models. *J. Atmos. Sci.*, **58**, 3224–3242.
- Ellingson, R., and Y. Fouquart, 1991: The intercomparison of radiation codes used in climate models: An overview. *J. Geophys. Res.*, **96**, 8925–8927.
- , J. Ellis, and S. Fels, 1991: The intercomparison of radiation codes used in climate models: Long wave results. *J. Geophys. Res.*, **96**, 8929–8953.
- Grabowski, W., X. Wu, M. Moncrieff, and W. Hall, 1998: Cloud-resolving modeling of cloud systems during phase III of GATE. Part II: Effects of resolution and the third spatial dimension. *J. Atmos. Sci.*, **55**, 3264–3282.
- Han, D., and R. Ellingson, 2000: An experimental technique for testing the validity of cumulus cloud parameterizations for longwave radiation calculations. *J. Appl. Meteor.*, **39**, 1147–1159.
- Iacono, M., E. Mlawer, and S. A. Clough, 2000a: Application of a maximum-random cloud overlap method for RRTM to general circulation models. *Proc. 10th ARM Science Team Meeting*, San Antonio, TX, Atmospheric Radiation Measurement Program, 1–5.
- , —, S. Clough, and J. Morcrette, 2000b: Impact of an improved longwave radiation model, RRTM, on the energy budget and thermodynamic properties of the NCAR Community Climate Model. CCM 3. *J. Geophys. Res.*, **105**, 14 873–14 890.
- Kablick, G., III, 2008: Third intercomparison of radiation codes in climate models: Longwave cloudy sky benchmarks and comparisons with approximate methods. M.S. thesis, Dept. of Meteorology, The Florida State University. [Available online at <http://etd.lib.fsu.edu/theses/available/etd-07142008-111858/>.]
- Kuhn, W., 1978: The effects of cloud height, thickness, and overlap on tropospheric terrestrial radiation. *J. Geophys. Res.*, **83**, 1337–1346.
- Li, J., and H. W. Barker, 2005: A radiation algorithm with correlated- $K$  distribution. Part I: Local thermal equilibrium. *J. Atmos. Sci.*, **62**, 286–309.
- Marshak, A., and A. Davis, Eds., 2005: *3D Radiative Transfer in Cloudy Atmospheres*. Springer-Verlag, 686 pp.
- Mlawer, E., S. Taubman, P. Brown, M. Iacono, and S. Clough, 1997: Radiative transfer for inhomogeneous atmospheres: RRTM, a validated correlated- $k$  model for the longwave. *J. Geophys. Res.*, **102**, 16 663–16 882.
- Morcrette, J., H. Barker, J. Cole, M. Iacono, and R. Pincus, 2008: Impact of a new radiation package, McRad, in the ECMWF integrated forecasting system. *Mon. Wea. Rev.*, **136**, 4773–4798.
- National Research Council, 1982: *Carbon Dioxide and Climate: A Second Assessment*. National Academy Press, 72 pp.
- Pincus, R., and S. A. Klein, 2000: Unresolved spatial variability and microphysical process rates in large-scale models. *J. Geophys. Res.*, **105**, 27 059–27 065.
- , H. Barker, and J. Morcrette, 2003: A fast, flexible, approximate technique for computing radiative transfer in inhomogeneous

- cloud fields. *J. Geophys. Res.*, **108**, 4376, doi:10.1029/2002JD003322.
- , R. Hemler, and S. Klein, 2006: Using stochastically generated subcolumns to represent cloud structure in a large scale model. *Mon. Wea. Rev.*, **134**, 3644–3656.
- Räisänen, P., 1998: Effective longwave cloud fraction and maximum-random overlap of clouds: A problem and a solution. *Mon. Wea. Rev.*, **126**, 3336–3340.
- , H. Barker, M. Khairoutdinov, J. Li, and D. Randall, 2004: Stochastic generation of subgrid-scale cloudy columns for large-scale models. *Quart. J. Roy. Meteor. Soc.*, **130**, 2047–2067.
- Siebesma, A., and J. Cuijpers, 1995: Evaluation of parametric assumptions for shallow cumulus convection. *J. Atmos. Sci.*, **52**, 650–666.
- Stephens, G., 2005: Cloud feedbacks in the climate system: A critical review. *J. Climate*, **18**, 237–273.
- Stevens, B., and Coauthors, 2001: Simulations of trade wind cumuli under a strong inversion. *J. Atmos. Sci.*, **58**, 1870–1891.
- Stokes, G., and S. Schwartz, 1994: The Atmospheric Radiation Measurement (ARM) Program: Programmatic background and design of the cloud and radiation test bed. *Bull. Amer. Meteor. Soc.*, **75**, 1201–1221.
- Taylor, P., and R. Ellingson, 2008: A study of the probability of clear line of sight through single-layer cumulus cloud fields in the tropical western Pacific. *J. Atmos. Sci.*, **65**, 3497–3512.
- Turner, D., and Coauthors, 2004: The QME AERI LBLRTM: A closure experiment for downwelling high spectral resolution infrared radiance. *J. Atmos. Sci.*, **61**, 2657–2675.